Pyrene-Based AIE System: A Bridge Model to Regulate Aggregate Structures

Xu-Min Cai[a],[e],*,†, Yuting Lin[a],†, Jianyu Zhang[b],†, Zhenguo Tang[a], Shouji Li[a], Weiren Zhong[a], Ziyue Ye[c], Feng Gao[c], Wen-Jin Wang[c], Xing Feng[d], Zheng Zhao[c],*, Qiang Yong[a],* and Ben Zhong Tang[c],*

[a] Jiangsu Co-Innovation Center of Efficient Processing and Utilization of Forest Resources, International Innovation Center for Forest Chemicals and Materials, College of Chemical Engineering, Nanjing Forestry University, Nanjing 210037, China

[b] Stratingh Institute for Chemistry and Zernike Institute for Advanced Materials, University of Groningen, Nijenborgh 4, Groningen 9747 AG, The Netherlands

[c] School of Science and Engineering, Shenzhen Institute of Aggregate Science and Technology, The Chinese University of Hong Kong, Shenzhen (CUHK-Shenzhen), Guangdong 518172, P.R. China

[d] Guangdong Provincial Key Laboratory of Information Photonics Technology, School of Material and Energy, Guangdong University of Technology, Guangzhou 510006, P. R. China

[e] Guangdong Provincial Key Laboratory of Luminescence from Molecular Aggregates, Guangzhou 510640, China

KEYWORDS: Aggregation-induced emission; Pyrene; Aggregate structure; Fluorescence; Dynamic encryption-decryption

ABSTRACT: The bridging role of aggregate between single-molecule structures and macroscopic photophysical properties has attracted intense attention. Pyrene (Py), as the simplest dimer candidate, is a proper model for studying accurate structure-property relationships of aggregates. Herein, a series of Py and derivatives were systematically investigated. With a largely planar and conjugated conformation, Py shows anomalous aggregation-induced emission (AIE) characteristics due to the oxygen quenching at the molecular level but turn-on fluorescence in the aggregate state because of the oxygen isolation. Although introducing substituents induces molecular motion and weakened luminescence in the molecular state, the impact of substituents on the aggregate-state photophysical properties enormously differs. A small and electron-conjugated substituent (-CHO) can generate long-range ordered dimer stacking, leading to redshifted and weakened emission. Meanwhile, the larger substituent (-CyA) can disrupt long-range stacking and result in discrete dimers, leading to blue-shifted but enhanced emission. Further, incorporating a natural and bulky alicyclic structure (-DAA) inhibits dimer formation and activates strong molecular motions in the crystalline state, resulting in the shortest wavelength and weakest emission. Interestingly, crystalline Py-DAA exhibits both mechanochromic and acidichromic properties, which can be synergistically applied in dynamic encryption-decryption. These results indicate that substituents significantly affect their fluorescent behaviors due to the complexity of aggregate structures. This work not only elucidates the unique AIE performance of Py for the first time but also applies it as an accurate model for regulating the aggregate structures, offering precise molecular design strategies for aggregate-state luminescent materials.

INTRODUCTION

Traditional methodology on organic solid materials is based on the "reductionistic" approach, which holds the concept that the properties of the microscopic molecular structure can determine those of the macroscopic substance. Therefore, traditional material design usually focuses only on the properties at molecular level[1-3]. However, many facts have proved that this is not always true. For example, the solid-liquid-gas phases of water and the solid-gas states of carbon dioxide all represent the same molecular structure but different macroscopic properties. For typical luminogens, perylene and hexaphenylsilole (HPS) exhibit completely different fluorescence properties in both solution and aggregate states, which are referred to as aggregation-caused quenching (ACQ) and aggregation-induced emission (AIE) behaviors, respectively[4-5]. On this basis, it is proposed that a gap exists between molecular structure and material property, i.e., aggregate structure, which plays a bridging role in determining their different properties in different states[6-8]. However, due to the unclear structure-property relationships, the design and control of

https://doi.org/10.26434/chemrxiv-2024-xrtp1 **ORCID:** https://orcid.org/0000-0003-2567-213X Content not peer-reviewed by ChemRxiv. **License:** CC BY-NC-ND 4.0

aggregate structures remain challenging. Nevertheless, a "holistic" approach using specific aggregate structure systems as models to study the aggregation process through the macroscopic properties could be adopted, thus elucidating the corresponding aggregate structures. By investigating such a system, it is probable to achieve initial control of the macroscopic property at the aggregate level (Figure 1a).

Pyrene (Py) is a highly planar and conjugated molecule. Hence, it is prone to form a dimer structure due to strong π-π stacking during the aggregation process[9-11]. To our knowledge, dimer is the simplest form of aggregate structure. However, there are various types of dimer structures with distinct π-π distances and overlaps, which can be appropriately used as aggregate models to study the structure-property relationship at the aggregate level[12-15]. Kambe and coworkers introduced alkyl chains with different lengths and branching patterns into the Py scaffold and found the alkyl chain-position-dependent photophysical properties. The solid-state properties could be modulated by changing the alkyl groups to alter the crystal packing[12]. Li et al. described a simple and effective method to regulate distances in Py dimers via mono- and di-substitution, elucidating the clear correlations between Py distance and emission wavelength[13]. Elucidating the structure-property relationships in the aggregate state by these pioneering works is beneficial for conducting structural design at the molecular level, thereby providing more precise molecular design strategies for our purpose. This represents a typical "holistic" methodology.

In addition, factors affecting the photophysical properties of aggregates include molecular motion, substituents, oxygen, and aggregate structures. Substituents are often introduced to study the differences in the optical properties of aggregates, such as electron donor/acceptor, positional isomers, bulky/small substituents, etc. For instance, incorporating D/A groups intrigues the charge transfer process in the excited states, thus affecting the photophysical properties[16-17]. Meanwhile, isomeric positions influence the behaviors of aggregate structures due to the steric hindrance and conjugation effects[18-19]. Further, the size of the groups can affect the packing of aggregates by altering the steric hindrance, which in turn changes the properties of aggregates[20]. Frequently, traditional substituent selection relies on commonly used ones with regular structures, such as triphenylamine and tetraphenylethylene[21-22], leading to a shortage of originality in structural design. The novel structures derived from biomass, such as rosin, may bring new ideas for molecular design[23-29]. Based on our previous findings, the rigid alicyclic moiety of rosin can be used to restrict the intramolecular motion of the flexible chromophore of simple Schiff bases, leading to aggregated emission[30-31]. The unique and natural alicyclic structure as a substituent for Py may be a potential candidate for producing unexpected photophysical properties. Furthermore, oxygen is another critical factor affecting luminescence properties, especially when relevant to the triplet state[32-33]. Understanding the specific effects of these factors on aggregate states is of great significance for studying the structure-property relationships between molecular/aggregate structures and macroscopic properties.

Herein, a series of derivatives based on the Py skeleton were systematically investigated. With a largely planar and conjugated structure, Py exhibits anomalous AIE behavior due to the combined effect of oxygen and aggregation. In addition, the initial control of Py-dimer structures with the corresponding macroscopic fluorescence properties has been achieved by elucidating the factors, including oxygen, substituent, molecular motion, and aggregate structure at different levels of structural hierarchy. This work not only elucidates the unique AIE performance of Py for the first time but also applies it as an accurate bridging model for regulating aggregate structures from a "holistic" perspective (Figure 1b).

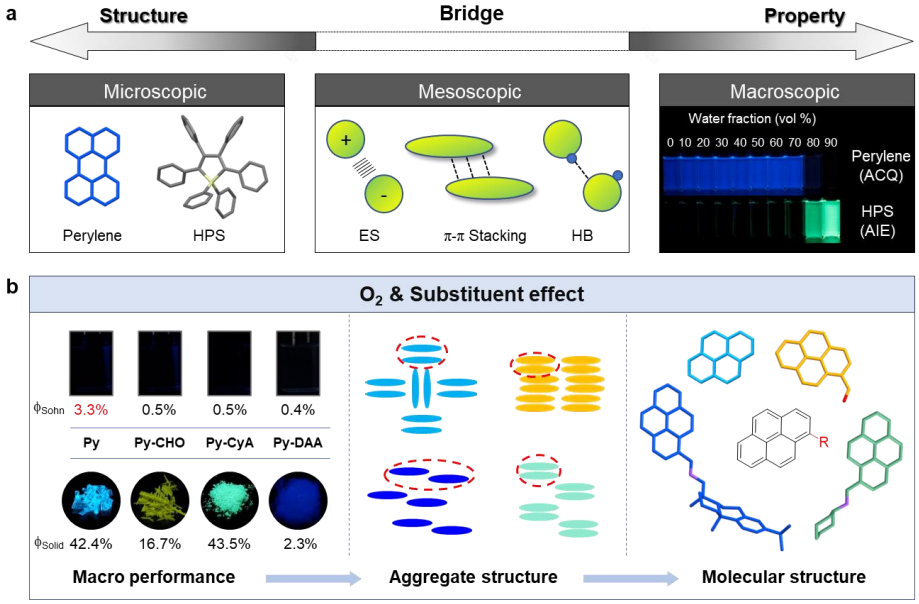

Figure 1. Schematic illustration of design approaches for the pyrene-based AIE system. ES and HB represent electrostatic effect and hydrogen bonding, respectively.

https://doi.org/10.26434/chemrxiv-2024-xrtp1 **ORCID:** https://orcid.org/0000-0003-2567-213X Content not peer-reviewed by ChemRxiv. **License:** CC BY-NC-ND 4.0

RESULTS AND DISCUSSION

As shown in Scheme S1, 1-Pyrenecarboxaldehyde (Py-CHO) reacted with Cyclohexylamine (CyA) and Dehydroabietylamine (DAA) via a simple Schiff base reaction to yield Py-CyA and Py-DAA. Structures were confirmed by ^{1}H and ^{13}C NMR and high-resolution mass spectroscopy measurements (Figures S1-S6). Single crystals of Py, Py-CHO, Py-CyA, and Py-DAA were obtained via slow evaporation for X-ray diffraction measurements (please see the details in the SI).

The photophysical properties of all four compounds were first studied. They all show the typical AIE effect with weak fluorescence in dilute solution and enhanced fluorescence at high water fraction (f_w) (Figure 2a). Among them, the AIE effect of Py challenges our previous knowledge of the traditional ACQ phenomenon, which always happens within planarly conjugated luminogens, driving us to find the underlying reasons for the opposite observation. From the photoluminescence (PL) spectra, Py exhibits fine-structured monomer emission in the molecular state (Figure 2b). As the f_w gradually increases, the emission intensity of the monomer rises due to the polarity of the solvent[14, 34]. When f_w > 80%, the intensity of the monomer peak decreases and is accompanied by a new and broad peak with visible sky-blue fluorescence, which is attributed to the dimer emission generated by aggregation[14]. With the increased concentration, the dimer-emission proportion of Py also increases (Figure S7), consistent with a previous report[14]. Still, they fail to provide a clear explanation for the following issue: although it is easy to understand that the AIE phenomenon originates from dimer emission, the monomer emission does not exhibit an ACQ phenomenon. The fact suggests that the emission in the molecular state may be influenced by factors other than polarity. According to the literature, the fluorescence of Py is always quenched by oxygen in the solvent[35-37]. Therefore, the PL spectra, absolute quantum yield (QY), and lifetime of Py in the molecular state before and after the degassing process were compared (Figure 2c and Table 1). After degassing, the PL intensity significantly increases, QY rises from 3.3% to 54.0%, and the lifetime also increases from 15.75 ns to 126.07 ns. The results indicate that oxygen indeed plays an essential role in the luminescent behaviors of Py. Accordingly, we also measured the PL spectra of Py in DMSO solution upon UV light irradiation (Figure 2d). The PL intensity increased with the elongated irradiation time, suggesting the generation of singlet oxygen during the irradiation process. Singlet oxygen can react with DMSO to gradually create an oxygen-free environment and enhance Py fluorescence[33]. The generation of singlet oxygen indicates the production of triplet excited states in Py, which was supported by the previous report [38-39]. Under oxygen-containing conditions, the triplet excitons react with oxygen, resulting in the non-radiative decay. However, under anaerobic conditions, the triplet excitons may undergo the triplet-triplet annihilation (TTA) process, leading to delayed fluorescence[13, 40-41] and increasing the PL intensity, QY, and lifetime. To further understand the evolution of excited states, we calculated the singlet and triplet energy levels of Py. As shown in Figure 2e, the energy level of S_1 (3.450 eV) is approximately twice that of T_1 (1.719 eV), meeting the basic conditions for TTA.

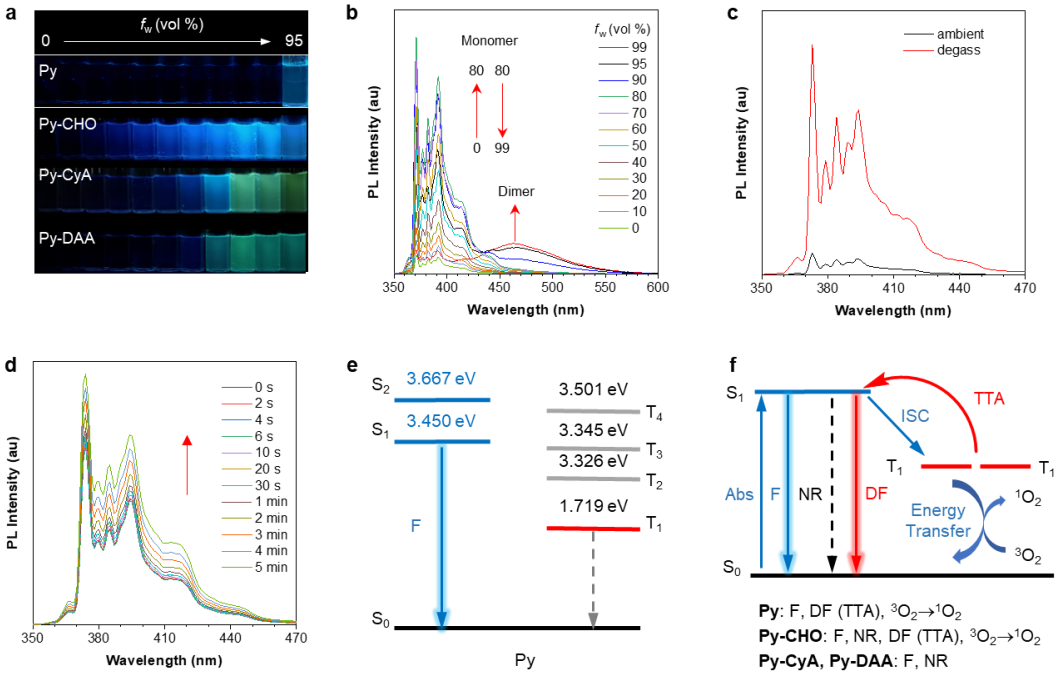

Figure 2. (a) Fluorescence photographs of Py, Py-CHO, Py-CyA, and Py-DAA in THF/H_2O mixtures with different f_w taken under a 365 nm UV lamp. Concentration: 20 μM. (b-d) PL spectra of Py in (b) THF/H_2O mixtures with different f_w, (c) the ambient and degassed states, and (d) DMSO solution upon UV light irradiation. Concentration: 20 μM; λ_{ex} = 335 nm. (e) The calculated energy levels of Py. (f) A simplified Jablonski diagram to illustrate the photophysical processes. Abs is absorption, F is fluorescence, NR is non-radiative relaxation, DF is delayed fluorescence, ISC is intersystem crossing, and TTA is triplet–triplet annihilation.

https://doi.org/10.26434/chemrxiv-2024-xrtp1 **ORCID:** https://orcid.org/0000-0003-2567-213X Content not peer-reviewed by ChemRxiv. **License:** CC BY-NC-ND 4.0

Table 1. Summary of photophysical properties of Py, Py-CHO, Py-CyA, and Py-DAA in solution, aggregate, and crystal state.

Comp.	λ_{ab} [nm]	λ_{em} [nm]		Φ_F [%]		τ [ns]		λ_{em} [nm] (Aggr, f_w = 95%)	Φ_F [%] (Aggr, f_w = 95%)	λ_{em} [nm] (Cryst)	Φ_F [%] (Cryst)
	Soln [a]	Soln [a]	Soln [b]	Soln [a]	Soln [b]	Soln [a]	Soln [b]				
Py	335	373	373	3.3	54.0	15.75	126.07	371, 465	27.0	465	42.4
Py-CHO	360	391	387	0.5	9.4	7.17	12.28	469	41.5	543	16.7
Py-CyA	360	391	391	0.5	0.8	NA	NA	507	35.1	495	43.5
Py-DAA	360	392	392	0.4	0.5	NA	NA	500	15.8	422	2.3

[a] in THF solution (20 μM) with air
[b] in degassed THF solution (20 μM)

Besides, the molecular state of Py-CHO is also influenced by oxygen (Table 1 and Figure S8), with a lower QY of only 0.5% under oxygen-containing conditions than Py. This may be related to molecular motion and n-π* transitions. After degassing, the QY of Py-CHO increased to 9.4%, along with an increase in the lifetime from 7.17 to 12.28 ns, exhibiting a similar trend as Py. From the energy levels of singlet and triplet states, Py-CHO also satisfies the possibility for TTA (Figure S9). On the contrary, Py-CyA and Py-DAA show very low QY and lifetime in their molecular states before and after degassing without noticeable delayed fluorescence, which may be attributed to the dominant molecular motions introduced by the largely flexible substituents (CyA and DAA), making the influence of oxygen negligible (Table 1 and Figure S8). Based on the above results, it is proposed that the excited-state processes experienced by Py in the molecular state include fluorescence, DF of TTA, and energy transfer. The substitution of the aldehyde group could introduce molecular motions into the rigid molecular skeleton, leading to stronger non-radiative decay. When CyA and DAA are introduced, primary fluorescence and non-radiative processes occur due to the dominance of molecular motions (Figure 2f).

The detailed photophysical properties of Py under different f_w provide insights into the fundamental mechanism of weak molecular state emission and AIE properties of this conjugated planar compound. Although oxygen plays a vital role in the molecular state emission of Py, does oxygen impact the aggregate state? According to Figure 3a, after forming Py aggregates, there is an increase in dimer emission and an enhancement in monomer emission. Theoretically, the emission intensity from monomers should decrease significantly after aggregation due to the reduced proportion of monomers and increased energy transfer from monomers to dimers. The strange behavior of increased monomer emission suggests that aggregation may isolate oxygen, enabling monomers to avoid quenching and instead exhibit enhanced emission. Additionally, a different AIE trend of Py-CHO was observed compared to Py (Figure 3b). When f_w < 90%, the monomer emission is too weak to be noticed, and a continuous redshift enhancement is observed as the f_w increases. Its QY in the aggregate state reaches 41.5% (far exceeding the molecular state of 0.5%), indicating the combined proximity effect and aggregation[42]. Py-CyA and Py-DAA exhibit similar AIE trends to Py, wherein monomer emission is observed in the molecular state, and a new emission peak from dimer appears after aggregation (Figure 3c-d). The concentration and viscosity experiments also confirm their AIE properties (Figures S7 and S10). The difference lies in the dimer emission of the latter two compounds, which is much stronger than the monomer emission. This is because the molecule-state emission of Py-CyA and Py-DAA are extremely weak due to molecular motion. After aggregation, the restricted motions enhance fluorescence with increased QY from 0.5% to 35.1% of Py-CyA and 0.4% to 15.8% of Py-DAA, respectively.

Interestingly, the fluorescence of the crystals and aggregates (f_w = 95%) of the four compounds show significant differences (Figure 3e-i). The aggregated Py exhibits emission from both monomer and dimer, indicating the disordered packing after rapid aggregation. The emission peak of the dimer is consistent with that of the crystalline state with shift (Δ = 0), suggesting that the dimer structure of Py in the aggregate state is similar to the packing in the crystalline state. However, Py-CHO crystal is significantly redshifted compared to the aggregate state (Δ > 0), exhibiting yellow emission. On the other hand, the crystals of Py-CyA and Py-DAA exhibit varying degrees of blueshift compared to the aggregate state (Δ < 0), indicating that the dimer structures of the substituted Py derivatives in the aggregate state and crystal state differ to some extent. This difference may be attributed to the dominance of the electronic effect of the Py scaffold during the rapid formation of aggregates, favoring discrete dimers and resulting in sky-blue or green emission (wavelength range of 460-510 nm). In contrast, the substitution groups control the slow crystallization process, leading to dark blue emission of Py-DAA (422 nm), sky-blue emission of Py (465 nm), green emission of Py-CyA (495 nm), and yellow emission of Py-CHO (543 nm). The various fluorescence properties exhibited by the aggregate and crystalline states provide more insights into the critical influence of the dimer structure of the Py scaffold on the macroscopic luminescent properties. Understanding the structure-property relationship of the Py scaffold dimers is beneficial for inferring the aggregate state structure of compounds and making rational molecular designs through a "holistic" approach.

https://doi.org/10.26434/chemrxiv-2024-xrtp1 **ORCID:** https://orcid.org/0000-0003-2567-213X Content not peer-reviewed by ChemRxiv. **License:** CC BY-NC-ND 4.0

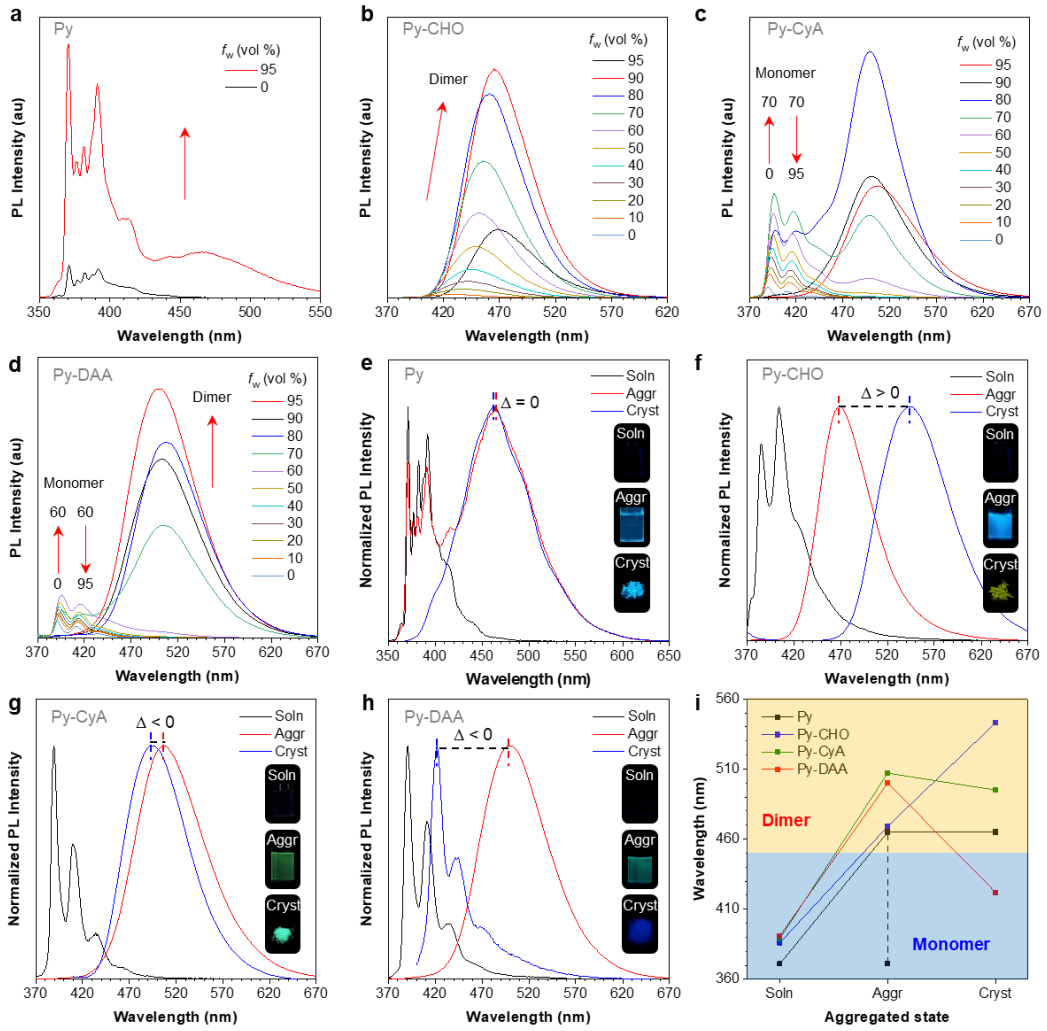

Figure 3. (a) PL spectra of Py in THF/H_2O mixtures with f_w = 0% and 95%. Concentration: 20 μM; λ_{ex} = 335 nm. (b-d) PL spectra of (b) Py-CHO, (c) Py-CyA, (d) Py-DAA in THF/H_2O mixtures with different f_w. Concentration: 20 μM; λ_{ex} = 360 nm. (e-h) PL spectra of (e) Py, (f) Py-CHO, (g) Py-CyA, and (h) Py-DAA in the solution, aggregate (f_w = 95%), and crystal states, respectively. Concentration: 20 μM. *Δ* represents the wavelength of the crystal minus the wavelength of the aggregate. (i) The plots of wavelength versus compounds in the solution (minimum wavelength), aggregate, and crystal states.

To further understand the structure-property relationship in the aggregate state, the single-crystal structures of these four compounds were obtained (Figure 4 and Table S1). As shown in Figure 4a, Py owns a planar conformation with a short distance (3.535 Å) and a large overlap (58%) between adjacent Py molecules, resulting in dimer emission. The stacking pattern indicates a discrete arrangement, which leads to strong sky-blue fluorescence with a QY of 42.4%. Similarly, Py-CHO possesses a relatively planar conformation (with a torsion angle of only 2.61°). Compared to Py, the distance between adjacent Py scaffolds in Py-CHO is smaller (3.475 Å), and the overlap is larger (62.5%), resulting in stronger π-π interactions. Additionally, the electronic effect brought by the aldehyde group endows Py-CHO with a head-to-tail and long-range ordered stacking, resulting in exciton diffusion and quenching. Therefore, Py-CHO shows weaker yellow fluorescence with a QY of 16.7% (Figure 4b). Py-CyA and Py-DAA with larger substituents exhibit torsion angles of 21.23° and 19.42°, respectively, causing conformational distortion. The stacking of Py-CyA with a smaller steric hindrance group is similar to Py. However, with a discrete dimer alternating arrangement but a large overlap (62.5%), Py-CyA exhibits redshifted green fluorescence with a QY of 43.5% (Figure 4c). In the case of Py-DAA with the bulky rosin group, significant steric hindrance and looser arrangement during crystallization are formed, resulting in almost no overlap of Py moieties in Py-DAA and the bluest and weakest fluorescence from its monomer (QY = 2.3%) (Figure 4d). From the above results on the structure-property relationship in the crystalline state, it can be concluded that substituents can regulate the structure and properties of Py aggregates. Bulky substituents can disperse the aggregate of Py, resulting in a blueshifted and weaker fluorescence. Middle steric substituents have minimal impact on the emission behavior of aggregate, while substituents with both planarity and electron effects can lead to redshifted and weaker fluorescence. This explicit structure-property relationship

https://doi.org/10.26434/chemrxiv-2024-xrtp1 **ORCID:** https://orcid.org/0000-0003-2567-213X Content not peer-reviewed by ChemRxiv. **License:** CC BY-NC-ND 4.0

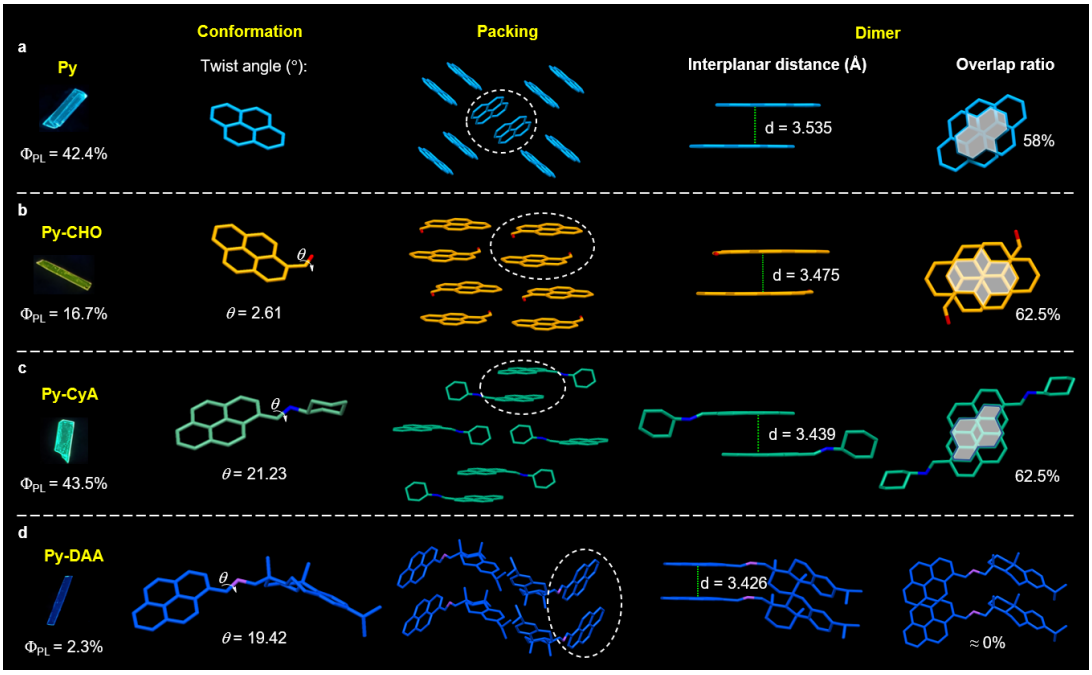

Figure 4. Molecular conformation, packing, and dimer of (a) Py (discrete dimer), (b) Py-CHO (long-range dimer), (c) Py-CyA (discrete dimer), and (d) Py-DAA (monomer).

in the aggregate state suggests that we can infer the aggregate structure of compounds and make rational molecular designs using a "holistic" approach.

The above discussion highlights the vital role of the aggregate structure in macroscopic properties. Therefore, it is possible to switch macroscopic properties by changing the aggregate structure under external stimuli. Taking Py-DAA as an example, the original sample exhibits a faint dark blue fluorescence. However, after grinding, it transforms into a bright green fluorescence (Figure 5a and 5b), showing significant mechanochromic luminescence (MCL) properties. PXRD spectra infer that the change in fluorescence color is due to the alteration of packing arrangement before and after grinding, which suggests that the Py units transition from a non-overlap state to a partial overlap state under the external force[14]. As expected, it successfully regulates macroscopic properties by modifying the aggregate structure[43]. However, fuming by volatile organic solvents or heating fails to restore it to the initial state because the strong π-π interactions between Py units could not be sufficiently disrupted. In addition, ground Py-DAA is sensitive to acid and base stimuli. When fuming with trifluoroacetic acid (TFA), its green fluorescence changes to red. Then, when fuming with triethylamine (TEA), it reverts to the original fluorescence with a dark blue color. Similarly, the above color change could also be achieved by fuming the crystalline sample with TFA and TEA vapors. NMR spectra illustrate that TFA protonates the imine bonds in Py-DAA[44-45] (Figures 5d and S11). The absorption spectra show that the protonated Py-DAA exhibits an additional absorption peak of charge-transfer (CT) state within 400-500 nm. Moreover, theoretical calculations based on density functional theory indicate that both HOMO and LUMO are located on the Py scaffold before the protonation of Py-DAA. After protonation, the significant CT process with a decreased energy gap is consistent with their redshifted emission. Py-CyA also exhibits the same ACL property (Figures S12-S13). Therefore, we can synergistically alter the macroscopic optical properties by separately altering the molecular and aggregate structure through external stimuli.

Stimuli-responsive materials have a wide range of applications in smart materials, such as anti-counterfeiting and encryption-decryption[46-47]. The multi-stimuli responsive properties of Py-DAA hold the potential to achieve dynamic encryption-decryption of information, thereby enhancing information security. Accordingly, we designed a quartz container to develop a dynamic encryption-decryption model as a proof-of-concept. Figure 6a represents the schematic diagram of the MCL and ACL properties of Py-DAA. The process involves placing the Py-DAA pristine powder in a quartz container, subjecting it to different treatments, such as grinding, fuming, and restoring it to its pristine state. The three states of Py-DAA and three commercial dyes with similar fluorescence color (lacking ACL properties) are filled in different positions of the quartz container and arranged in a specific order to achieve information storage. For example, the different states of the solid are filled in a 7×7 array of the quartz container, and information is written in this manner. Without any processing, the seemingly chaotic arrangement cannot provide valid information. However, by using TFA and TEA fumigation in order, two Chinese characters, "田" and "王", can be sequentially read, indicating that this model has dynamic decryption properties. This dynamic and color-controllable system also holds the potential to be a candidate material for three-dimensional (3D) code. The colorful 3D code is developed based on traditional two-dimensional codes with another dimension of color, demonstrating higher information storage capacity and better security.

https://doi.org/10.26434/chemrxiv-2024-xrtp1 **ORCID:** https://orcid.org/0000-0003-2567-213X Content not peer-reviewed by ChemRxiv. **License:** CC BY-NC-ND 4.0

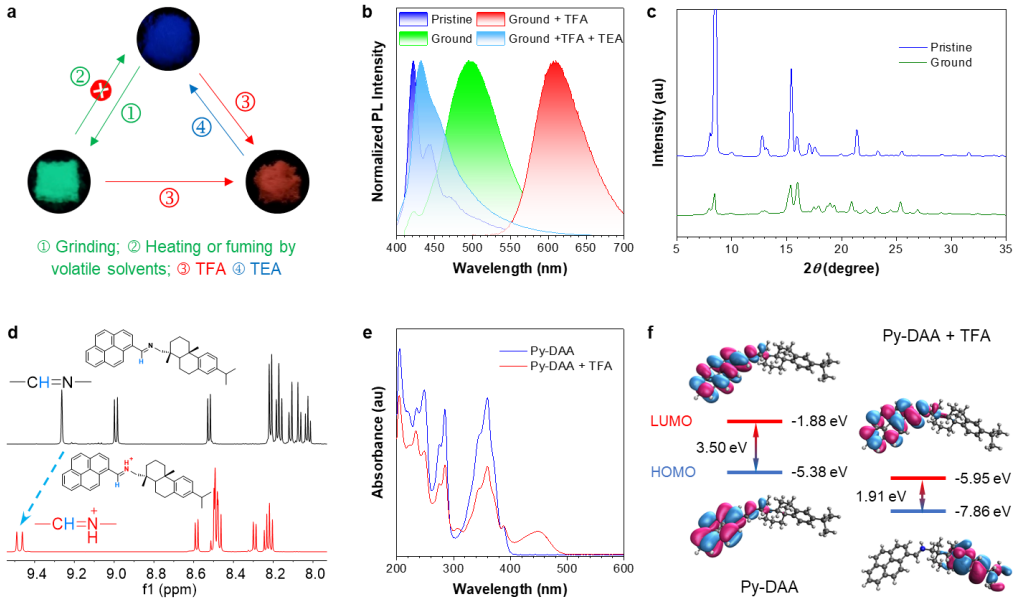

Figure 5. (a) Fluorescence photographs, (b) PL spectra, and (c) PXRD spectra of Py-DAA under various treatments. (d) NMR spectra of Py-DAA before and after the addition of TFA. (e) Absorption spectra of Py-DAA solid sample before and after fuming by TFA in pure EtOH solution. Concentration: 20 μM. (f) Frontier molecular orbitals and corresponding energy levels of Py-DAA before and after fuming by TFA.

This 3D code can be constructed by arranging a 5×5 quartz container with specific colors in a certain way (Figure 6d), and the number and arrangement of the four colors are controlled by different treatment methods of Py-DAA. For example, the encoding parsed into information A can dynamically be converted into the code pattern of "Rosin" through TFA fuming. After TEA fuming, it can be further dynamically switched to the third encoding, such as the new information code that can be analyzed as information C, showing the great potential of Py-DAA in constructing dynamic fluorescent 3D codes. Compared with traditional 3D codes that store information in a static form and do not support multi-level display of encrypted information, this dynamic and controllable multi-color fluorescent system may become a candidate for developing higher-level 3D codes and further enhancing information security. In addition, besides solids, Py-DAA solutions are also expected to be used as "invisible ink" for information storage and decryption (Figures S14 and S15). Information can be encrypted and selectively read by using it in combination with commercial ink. Compared with traditional single-stimulus response materials, the unique multi-stimulus response properties endow Py-DAA with better privacy and display the tremendous potential of this material in anti-counterfeiting and encryption-decryption applications.

CONCLUSION

The aggregate structures play a crucial bridging role in investigating the structure-property relationships of single -molecular structure and macroscopic photophysical properties. However, so far, the design of aggregate structures still faces challenges. In this work, Py has been adopted as an aggregate model to construct a series of derivatives by introducing substituents of -CHO, -CyA, and -DAA with different electronic and steric effects. The results demonstrate that rational molecular design can regulate the Py-based dimer structures, thereby controlling their macroscopic optical properties. With a largely planar and conjugated conformation, Py exhibits anomalous AIE properties resulting from the combination of oxygen and aggregation. The highly unexpected small QY of 3.31% at the molecular level uncovers that oxygen quenches the triplet exciton, leading to efficient non-radiative decay in the monomer state. However, aggregation can isolate oxygen, resulting in dimer emission and increased QY. Although introducing substituents induces molecular motion and weakens the emission intensity in the monomer state, their influence on the aggregate-state fluorescence properties is totally distinct. The introduction of a small and electronically conjugated substituent (-CHO) leads to long-range ordered stacking, resulting in redshifted and weakened emission. On the other hand, the larger substituent (-CyA) disrupts long-range stacking, resulting in discrete dimers with blue-shifted and enhanced emission close to those of the Py skeleton. Incorporating the bulky natural rosin structure (-DAA) with steric hindrance leads to the monomer mode in the crystalline state, resulting in intense molecular motion with the bluest and weakest emission. Furthermore, the aggregate structures can be changed by multiple external stimuli. Interestingly, Py-DAA exhibits MCL property due to changes in the aggregate structure under external force, while the protonation of imine bonds leads to ACL property. The synergistic effect of MCL and ACL provides excellent potential in dynamic encryption and decryption of information. This work not only clarifies the anomalous AIE property of Py, but also provides a precise bridging model to study the structure-property relationship at the aggregate level, thus offering more accurate molecular design strategies for aggregate-state luminescent materials from the "holistic" point of view.

https://doi.org/10.26434/chemrxiv-2024-xrtp1 **ORCID:** https://orcid.org/0000-0003-2567-213X Content not peer-reviewed by ChemRxiv. **License:** CC BY-NC-ND 4.0

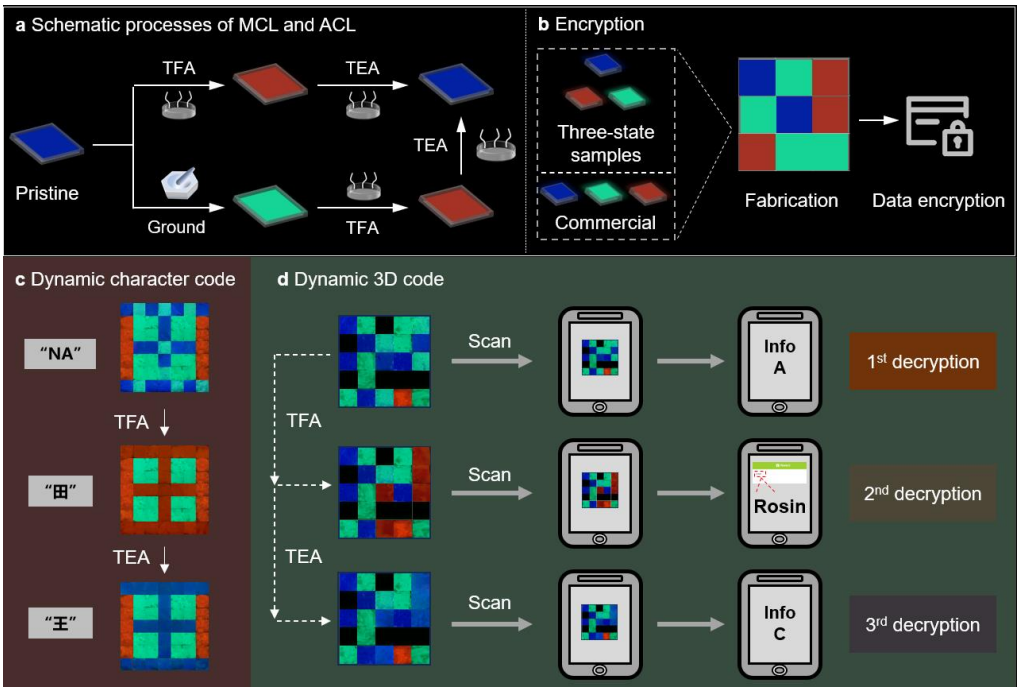

Figure 6. (a) Schematic progress of MCL and ACL of Py-DAA. (b) Schematic representations of the formation by adding Py-DAA under various treatments to quartz containers. Blue, green, and red represent the pristine sample, ground sample, and sample fumed by TFA of Py-DAA, and commercial dyes of their corresponding colors, respectively. (c-d) A schematic illustration of the information encryption-decryption process as character code (c) and 3D code (d).

ASSOCIATED CONTENT

Supporting Information.

The Supporting Information is available free of charge

Experimental details, NMR, MS, additional photophysical data (PDF)

AUTHOR INFORMATION

Corresponding Author

Xu-Min Cai – Jiangsu Co-Innovation Center of Efficient Processing and Utilization of Forest Resources, International Innovation Center for Forest Chemicals and Materials, Nanjing Forestry University, College of Chemical Engineering, Nanjing 210037, China; Guangdong Provincial Key Laboratory of Luminescence from Molecular Aggregates, Guangzhou 510640, China; Email: xumin.cai@njfu.edu.cn

Zheng Zhao – School of Science and Engineering, Shenzhen Institute of Aggregate Science and Technology, The Chinese University of Hong Kong, Shenzhen (CUHK-Shenzhen), Guangdong 518172, P.R. China; Email: zhaozheng@cuhk.edu.cn

Qiang Yong – Jiangsu Co-Innovation Center of Efficient Processing and Utilization of Forest Resources, International Innovation Center for Forest Chemicals and Materials, Nanjing Forestry University, College of Chemical Engineering, Nanjing 210037, China; Email: swhx@njfu.com.cn

Ben Zhong Tang – School of Science and Engineering, Shenzhen Institute of Aggregate Science and Technology, The Chinese University of Hong Kong, Shenzhen (CUHK-Shenzhen), Guangdong 518172, P.R. China; Email: tangbenz@cuhk.edu.cn

Author Contributions

†X.-M. Cai, Y. Lin, and J. Zhang contributed equally to this paper.

Notes

The authors declare no competing financial interest.

ACKNOWLEDGMENT

Support from the National Natural Science Foundation of China (21601087), the Natural Science Foundation of Jiangsu Province (BK20231296), the Open Fund of Guangdong Provincial Key Laboratory of Luminescence from Molecular Aggregates, Guangzhou 510640, China (South China University of Technology (2023B1212060003)), the Shenzhen Key Laboratory of Functional Aggregate Materials (ZDSYS20211021111400001), the Science Technology Innovation Commission of Shenzhen Municipality (KQTD20210811090142053), and the Key Research and Development Project of Yunnan Province (202303AC100010). J. Zhang acknowledges the support from the European Union's Horizon 2020 research and innovation program under the Marie Skłodowska-Curie actions grant (101105790). We also thank the AIE Institute (www.aietech.org.cn) for providing some AIE materials and technical assistance as well as Professor Zhipeng Liu for valuable discussions.

REFERENCES

(1) Tang, B. Z. Aggregology: Exploration and innovation at aggregate level. *Aggregate* **2020,** *1* (1), 4-5.

(2) Tu, Y.; Zhao, Z.; Jacky, W.; Tang, B. Aggregate Science: Much to Explore in the Meso World. *Matter* **2021,** *4*, 338-349.

(3) He, W.; Kwok, R. T. K.; Qiu, Z.; Zhao, Z.; Tang, B. Z. A Holistic Perspective on Living Aggregate. *J. Am. Chem. Soc.* **2024,** *146* (8), 5030-5044.

(4) Yang, J.; Fang, M.; Li, Z. Organic luminescent materials: The concentration on aggregates from aggregation-induced emission. *Aggregate* **2020,** *1* (1), 6-18.

(5) Mei, J.; Leung, N. L. C.; Kwok, R. T. K.; Lam, J. W. Y.; Tang, B. Z. Aggregation-Induced Emission: Together We Shine, United We Soar! *Chem. Rev.* **2015,** *115* (21), 11718-11940.

https://doi.org/10.26434/chemrxiv-2024-xrtp1 **ORCID:** https://orcid.org/0000-0003-2567-213X Content not peer-reviewed by ChemRxiv. **License:** CC BY-NC-ND 4.0

(6) Zhang, H.; Zhao, Z.; Turley, A. T.; Wang, L.; McGonigal, P. R.; Tu, Y.; Li, Y.; Wang, Z.; Kwok, R. T. K.; Lam, J. W. Y.; Tang, B. Z. Aggregate Science: From Structures to Properties. *Adv. Mater.* **2020,** *32* (36), 2001457.
(7) Li, Q.; Li, Z. Molecular Packing: Another Key Point for the Performance of Organic and Polymeric Optoelectronic Materials. *Acc. Chem. Res.* **2020,** *53* (4), 962-973.
(8) Li, Q.; Li, Z. The Strong Light-Emission Materials in the Aggregated State: What Happens from a Single Molecule to the Collective Group. *Adv. Sci.* **2017,** *4* (7), 1600484.
(9) Robertson, J. M.; White, J. G. The crystal structure of pyrene. A quantitative X-ray investigation. *J. Chem. Soc.* **1947,** 358-368.
(10) Fang, M.; Yang, J.; Li, Z. Light emission of organic luminogens: Generation, mechanism and application. *Prog. Mater Sci.* **2022,** *125*, 100914.
(11) Feng, X.; Wang, X.; Redshaw, C.; Tang, B. Z. Aggregation behaviour of pyrene-based luminescent materials, from molecular design and optical properties to application. *Chem. Soc. Rev.* **2023,** *52* (19), 6715-6753.
(12) Iwasaki, T.; Murakami, S.; Takeda, Y.; Fukuhara, G.; Tohnai, N.; Yakiyama, Y.; Sakurai, H.; Kambe, N. Molecular Packing and Solid-State Photophysical Properties of 1,3,6,8-Tetraalkylpyrenes. *Chem. Eur. J.* **2019,** *25* (65), 14817-14825.
(13) Wang, J.; Dang, Q.; Gong, Y.; Liao, Q.; Song, G.; Li, Q.; Li, Z. Precise Regulation of Distance between Associated Pyrene Units and Control of Emission Energy and Kinetics in Solid State. *CCS. Chem.* **2021,** *3* (12), 274-286.
(14) Gong, Y.-B.; Zhang, P.; Gu, Y.-r.; Wang, J.-Q.; Han, M.-M.; Chen, C.; Zhan, X.-J.; Xie, Z.-L.; Zou, B.; Peng, Q.; Chi, Z.-G.; Li, Z. The Influence of Molecular Packing on the Emissive Behavior of Pyrene Derivatives: Mechanoluminescence and Mechanochromism. *Adv. Optical Mater.* **2018,** *6* (16), 1800198.
(15) Gong, Y.; He, S.; Li, Y.; Li, Z.; Liao, Q.; Gu, Y.; Wang, J.; Zou, B.; Li, Q.; Li, Z. Partially Controlling Molecular Packing to Achieve Off–On Mechanochromism through Ingenious Molecular Design. *Adv. Optical Mater.* **2020,** *8* (8), 1902036.
(16) Jiang, Z.; Liang, Z.; Cui, Y.; Zhang, C.; Wang, J.; Wang, H.; Wang, T.; Chen, Y.; He, W.; Liu, Z.; Guo, Z. Blood–Brain Barrier Permeable Photoacoustic Probe for High-Resolution Imaging of Nitric Oxide in the Living Mouse Brain. *J. Am. Chem. Soc.* **2023,** *145* (14), 7952-7961.
(17) Wang, X.; Jiang, Z.; Liang, Z.; Wang, T.; Chen, Y.; Liu, Z. Discovery of BODIPY J-aggregates with absorption maxima beyond 1200 nm for biophotonics. *Sci. Adv.* **2022,** *8* (48), eadd5660.
(18) Xiong, Y.; Zhao, Z.; Zhao, W.; Ma, H.; Peng, Q.; He, Z.; Zhang, X.; Chen, Y.; He, X.; Lam, J. W. Y.; Tang, B. Z. Designing Efficient and Ultralong Pure Organic Room-Temperature Phosphorescent Materials by Structural Isomerism. *Angew. Chem. Int. Ed.* **2018,** *57* (27), 7997-8001.
(19) Deng, H.; Yang, Z.; Li, G.; Ma, D.; Xie, Z.; Li, W.; Mao, Z.; Zhao, J.; Yang, Z.; Zhang, Y.; Chi, Z. Dynamic organic mechanoluminescence (ML): The roles of Mechano-induced conformational isomer and energy transfer from ML to photoluminescence (PL). *Chem. Eng. J.* **2022,** *438*, 135519.
(20) Cai, X.-M.; Tang, Z.; Chen, X.; Lin, Y.; Zhang, X.; Huang, S. Construction of two rosin-based BioAIEgens with distinct fluorescence and mechanochromic propertites for rewritable paper. *Dyes Pigments* **2022,** *204*, 110454.
(21) Shang, A.; Lu, T.; Liu, H.; Du, C.; Liu, F.; Jiang, D.; Min, J.; Zhang, H.; Lu, P. Study of configuration differentia and highly efficient deep-red thermally activated delayed fluorescent organic light-emitting diodes based on phenanthro[4,5-fgh]quinoxaline derivatives. *J. Mater. Chem. C* **2021,** *9* (23), 7392-7399.
(22) Yang, J.; Li, L.; Yu, Y.; Ren, Z.; Peng, Q.; Ye, S.; Li, Q.; Li, Z. Blue pyrene-based AIEgens: inhibited intermolecular π–π stacking through the introduction of substituents with controllable intramolecular conjugation, and high external quantum efficiencies up to 3.46% in non-doped OLEDs. *Mater. Chem. Front.* **2017,** *1* (1), 91-99.
(23) Cai, X.-M.; Li, S.; Wang, W.-J.; Lin, Y.; Zhong, W.; Yang, Y.; Kühn, F. E.; Li, Y.; Zhao, Z.; Tang, B. Z. Natural Acceptor of Coumarin-Isomerized Red-Emissive BioAIEgen for Monitoring Cu^{2+} Concentration in Live Cells via FLIM. *Adv. Sci* **2023,** *11*, 2307078.
(24) Liu, W.; Pang, B.; Zhang, M.; Lv, J.; Xu, T.; Bai, L.; Cai, X.-M.; Yao, S.; Huan, S.; Si, C. Pickering multiphase materials using plant-based cellulosic micro/nanoparticles. *Aggregate* **2024,** *5*, e486.
(25) Wang, Y.; Xu, T.; Liu, K.; Zhang, M.; Cai, X.-M.; Si, C. Biomass-based materials for advanced supercapacitor: principles, progress, and perspectives. *Aggregate* **2024,** *5* (1), e428.
(26) Xu, K.; Gao, L.; Liang, Y.; Meng, Z.; Gong, S.; Wang, Z.; Wang, S. A ratiometric near-infrared fluorescent probe with a large Stokes shift for rapid and sensitive detection of hydrogen sulfide in food samples and imaging in biological system. *J. Food Compos. Anal.* **2024,** *127*, 106005.
(27) Lv, B.; Chen, L.; Wang, Z.; Zheng, Y.; Cui, Z.; Wu, Y.; Li, J.; Gu, W. A novel ratiometric tanshinone IIA-based fluorescent probe for sensitive and reversible detection of BF3 in solution and gaseous phase. *Tetrahedron* **2024,** *152*, 133821.
(28) Sun, L.; Wang, Z.; Chen, L.; Sun, X.; Yang, Z.; Gu, W. A novel dehydroabietic acid-based multifunctional fluorescent probe for the detection and bioimaging of Cu^{2+}/Zn^{2+}/ClO^{-}. *Analyst* **2023,** *148* (8), 1867-1876.
(29) Liu, Q.-s.; Yang, Z.-h.; Wang, Z.-l.; Sun, Y.; Chen, L.-l.; Sun, L.; Sun, X.-b.; Gu, W. A novel dehydroabietic acid-based AIE-active fluorescent probe for rapid detection of Hg^{2+} and its environmental and biological applications. *J. Photo. Photobio. A* **2022,** *423*, 113597.
(30) Cai, X.-M.; Lin, Y.; Li, Y.; Chen, X.; Wang, Z.; Zhao, X.; Huang, S.; Zhao, Z.; Tang, B. Z. BioAIEgens derived from rosin: how does molecular motion affect their photophysical processes in solid state? *Nat. Commun.* **2021,** *12* (1), 1773.
(31) Cai, X.-M.; Lin, Y.; Tang, Z.; Zhang, X.; Mu, T.; Huang, S.; Zhao, Z.; Tang, B. Z. Filling the gap between molecular and aggregate states: how does molecular packing affect photophysical properties? *Chem. Eng. J.* **2023,** *451*, 138627.
(32) Liu, D.; Zhang, M.; Tian, W.; Jiang, W.; Sun, Y.; Zhao, Z.; Tang, B. Z. Molecular core–shell structure design: Facilitating delayed fluorescence in aggregates toward highly efficient solution-processed OLEDs. *Aggregate* **2022,** *3* (2), e164.
(33) Jin, Y.; Peng, Q.-C.; Li, S.; Su, H.-F.; Luo, P.; Yang, M.; Zhang, X.; Li, K.; Zang, S.-Q.; Tang, B. Z.; Mak, T. C. W. Aggregation-induced barrier to oxygen—a new AIE mechanism for metal clusters with phosphorescence. *Natl. Sci. Rev.* **2021,** *9* (8), nwab216.
(34) Kalyanasundaram, K.; Thomas, J. K. Environmental effects on vibronic band intensities in pyrene monomer fluorescence and their application in studies of micellar systems. *J. Am. Chem. Soc.* **1977,** *99* (7), 2039-2044.
(35) Förster, T.; Kasper, K. Ein Konzentrationsumschlag der Fluoreszenz des Pyrens. *Z. Phys. Chem.* **1955,** *59* (10), 976-980.
(36) Parker, C. A.; Hatchard, C. G., Lifetime of the Pyrene Dimer. *Nature* **1961,** *190* (4771), 165-166.
(37) Basu, B. J.; Rajam, K. S. Comparison of the oxygen sensor performance of some pyrene derivatives in silicone polymer matrix. *Sens. Actuators B: Chem.* **2004,** *99* (2), 459-467.
(38) Parker, C. A.; Hatchard, C. G.; Bowen, E. J. Delayed fluorescence from solutions of anthracene and phenanthrene. *Proc. R. Soc. Lond. A* **1962,** *269* (1339), 574-584.
(39) Parker, C. A.; Hatchard, C. G. Delayed fluorescence of pyrene in ethanol. *Trans. Faraday Soc.* **1963,** *59* (0), 284-295.
(40) Ieuji, R.; Goushi, K.; Adachi, C. Triplet–triplet upconversion enhanced by spin–orbit coupling in organic light-emitting diodes. *Nat. Commun.* **2019,** *10* (1), 5283.
(41) Han, P.; Xia, E.; Qin, A.; Tang, B. Z. Adjustable and smart AIEgens for nondoped blue and deep blue organic light-emitting diodes. *Coord. Chem. Rev.* **2022,** *473*, 214843.
(42) Zhang, J.; Tu, Y.; Shen, H.; Lam, J. W. Y.; Sun, J.; Zhang, H.; Tang, B. Z. Regulating the proximity effect of heterocycle-containing AIEgens. *Nat. Commun.* **2023,** *14* (1), 3772.
(43) Zhang, J.; He, B.; Wu, W.; Alam, P.; Zhang, H.; Gong, J.; Song, F.; Wang, Z.; Sung, H. H. Y.; Williams, I. D.; Wang, Z.; Lam, J. W. Y.; Tang, B. Z. Molecular Motions in AIEgen Crystals: Turning on Photoluminescence by Force-Induced Filament Sliding. *J. Am. Chem. Soc.* 2020, 142 (34), 14608-14618.

https://doi.org/10.26434/chemrxiv-2024-xrtp1 **ORCID:** https://orcid.org/0000-0003-2567-213X Content not peer-reviewed by ChemRxiv. **License:** CC BY-NC-ND 4.0

(44) Xiong, Y.; Zhong, W.; Zhang, X.; Lin, Y.; Tang, Z.; Li, S.; Cai, X.-M. Dehydroabietic acid and triphenylamine combined BioAIEgens with an imine linker and RIM: mechanochromism and acidichromism. *Dyes Pigments* **2023,** *218*, 111475.
(45) Zhong, W.; Zhang, J.; Lin, Y.; Li, S.; Yang, Y.; Wang, W.-J.; Si, C.; Kühn, F. E.; Zhao, Z.; Cai, X.-M.; Tang, B. Z. Multi-site isomerization of synergistically regulated stimuli-responsive AIE materials toward multi-level decryption. *Chem. Sci.* **2024**, *15,* 3920-3927.
(46) Zhang, J.; He, B.; Hu, Y.; Alam, P.; Zhang, H.; Lam, J. W. Y.; Tang, B. Z. Stimuli-Responsive AIEgens. *Adv. Mater.* **2021,** *33* (32), 2008071.
(47) Yu, X.; Zhang, H.; Yu, J. Luminescence anti-counterfeiting: From elementary to advanced. *Aggregate* **2021,** *2* (1), 20-34.

https://doi.org/10.26434/chemrxiv-2024-xrtp1 **ORCID:** https://orcid.org/0000-0003-2567-213X Content not peer-reviewed by ChemRxiv. **License:** CC BY-NC-ND 4.0

For Table of Contents only

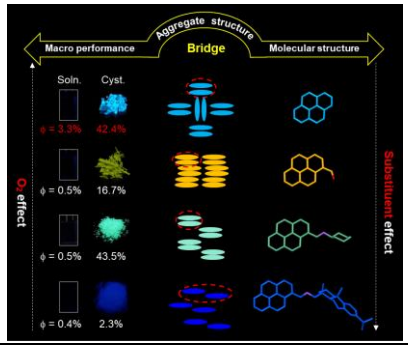

https://doi.org/10.26434/chemrxiv-2024-xrtp1 **ORCID:** https://orcid.org/0000-0003-2567-213X Content not peer-reviewed by ChemRxiv. **License:** CC BY-NC-ND 4.0